Journal of Applied Sciences and Nanotechnology

BTX Photodegradation Using Synthetic Nano Photocatalysts

[1]Firdos M. Abdulla*, [1]Zainab Y. Shnain, [1]Asawer A. Alwaisit, [2]Mohammad F. Abid

[1]Department of Chemical Engineering, University of Technology - Iraq, Iraq
[2]Department of Oil and Gas Refining Engineering, Al-Turath University College, Iraq

ARTICLE INFO

Corresponding Author:
Firdos M. Abdulla
firdos.m.abdulla@uotechnology.edu.iq

ABSTRACT

A photocatalytic tapered bubble column reactor was utilized to extract benzene, toluene, and xylene (BTX) organic pollutants from petroleum effluent. The reactor had an internal diameter that increased from 0.07 meters at the bottom to 0.17 meters at the top, a tapered angle of 1.6 degrees, a length of 1.8 meters, and a capacity of approximately 20 liters. Additionally, the reactor was equipped with a Fe-doped TiO_2 catalyst. Different air flow rates (0-3 L/min), contact periods (0-120 min), and liquid flow rates (160-600 L/hr) were used in the photocatalyst with four submerged LED lamps (wavelength of 200–550 nm). Each of the LED lamps had a power output of 50W. The results show that increasing the liquid flow rate increases the rate removal of COD, and the maximum decrease in chemical oxygen demand (COD) was 92% when gas flow rate= 3L/min, liquid flow rate = 200L/min, light intensity = 200Watt after two hours of irradiation. The kinetic study reveals that the degradation process is fitted with a pseudo first-order model with (R^2=0.9304, s.d. 0.00204).

1. Introduction

Oil and grease, alkanes, olefins, polycyclic aromatic hydrocarbons (PAHs), benzene, toluene, and xylene (BTX), mercaptans, phenol, ammonia, and a wide range of other organic compounds are among the contaminants that significantly contaminate the water that is produced which is also referred to as petroleum wastewater. There is also a high concentration of total solids, a high need for chemical and biological oxygen, and a high biological and chemical oxygen demand [1-3]. Developed oxidation processes (AOPs), membrane-based methods, biological treatments, and adsorption techniques are the four technologies that have advanced in terms of potential for ultimate wastewater treatment. The bulk of pollutants may be broken down into mineralized forms via biological and sophisticated oxidation processes. Adsorption and membrane processes transfer pollutants to various concentrated forms [3-5].

The photocatalytic procedure is capable of removing organic compounds that are difficult to being treated by biological method. TiO_2-based photocatalysts often treat organic pollutants and wastewater from the oil and gas industry. Because of its high catalytic efficiency, stability, and nontoxicity, the TiO_2/UV method has attracted much attention in photocatalysis since it was first introduced. Comprehensive mineralization of petroleum effluent is provided at a low cost, with rapid response times, no sludge generation, and an easy-to-use interface [2, 3, 6-8].

For pure titanium dioxide, the bandgaps of the anatase and rutile crystal forms are 3.2 and 3.6 eV, respectively. To increase the electrochemical and photochemical activity, it is possible to dope many kinds of ions made of transition metals such as Cr, Fe, V, Mn, Co, and Ni. These metals will provide additional energy levels to the bandgap, effectively reducing it so that it falls within the visible range [8-20]. To produce good photocatalysis, it is necessary to have a pollutant, an active catalyst, and an effective source of illumination in very close proximity to one another [21-23]. Using bubble columns, slurry bubble columns, and a three-phase fluidized reactor, the photocatalytic approach for treating wastewater has been the focus of various research [24, 25]. These investigations have included the use of bubble columns. However, the use of tapered bubble columns in the photocatalyst process has not been investigated. This work aims to study the effectiveness of semi-batch tapered bubble columns in the degradation of BTX using TiO_2 nanoparticles and Fe-doped TiO_2 catalysts under different flow rates of water and air and irradiation time.

2. Materials and methods

2.1. Materials

Experiments in the laboratory were carried out using samples of petroleum waste water that had been prepared. The chemical oxygen required (COD) was determined at this stage, corresponding to a catalyst dose of 50mg/L. Other specifications were pH: 6.5, contact time: 0-120min, and light intensity 200W. The wastewater sample pH was set using Sulfuric acid and sodium hydroxide solutions. The chemical materials utilized in the experimental work are listed and described in Table 1.

Table 1: Materials specifications.

Chemicals	Melting point ^oC	Density g/cm^3	Boiling point ^oC	Mol. Weight (g/mol)	Molecular formula	Country	Purity (%)
Benzene	5.53	0.876	80.1	78.11	C_6H_6	UK	99.5
Toluene	-95	0.867	110.6	92.14	$C_6H_5CH_3$	India	99.5
Xylene	-47.87	0.87	140	106.16	C_8H_{10}	India	99
Titanium dioxide	1843	4.26	2972	79.9	TiO_2	USA	99.9
Ferric Chloride	307.6	0.91	316	162.2	$FeCl_3$	India	99

2.2. Experimental Setup

The schematic and the image of the experimental setup are shown in Fig. 1 and 2, respectively. The test section is a tapered bubble column constructed of Plexiglas® with an internal diameter raised from 0.07 m at the bottom to 0.17 m at the top, a tapered angle of 1.6 o, a 1.8-meter length, and a capacity of about 20 L. A compressor (type: supper compressor, 120LT) provides air to the test area. A perforated sinter element with an average pore size of 1 mm and 91 holes is underneath the mixing chamber of the lower plenum. The experiments were conducted at room temperature and kept constant during the experiments using a water cooler.

Four 50W-LED lamps placed in the center of the reactor within a 25 mm-diameter quartz tube irradiated the photocatalysis degradation process of BTX. The lamps were completely submerged in the reactor, allowing optimum light usage.
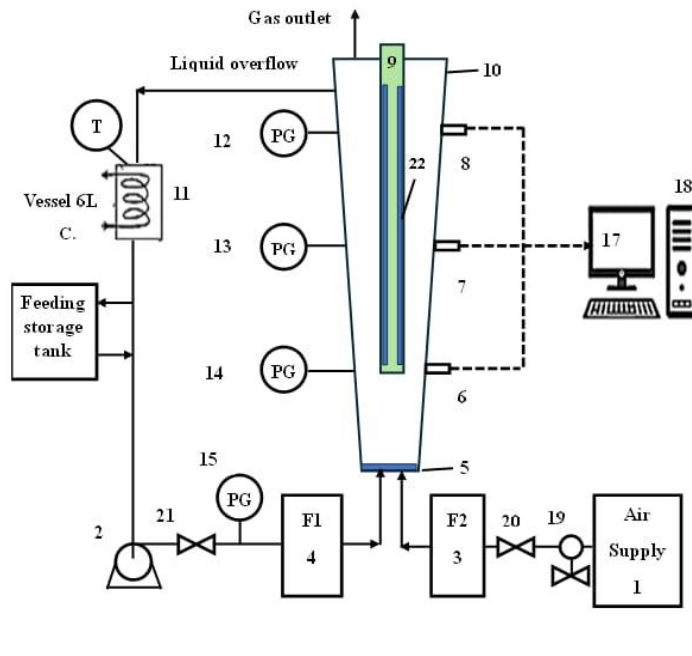
Item No.	Description
1	Air supply(compressor)
2	Water pump
3	Gas flowmeter
4	Liquid flow meter
5	Micro bubble distributer (91 Holes, 1mm Di. of each hole)
6 to 8	Conductivity probe1,2,3
9	Quartz glass pipe
10	Tapered column (1.8m height, 0.07m at the bottom to 0.17m at the top)
11	Heat exchanger
12 to 15	Pressure gage
16	Feeding storge tank
17	Laptop for data record
18	data acquisition
19	Air filter regulator
20	Liquid flow control valve
21	Gas flow control valve
22	LED lamps

Figure 1: Preliminary schematic of the experimental setup.

Figure 2: The experimental setup Photograph.

2.3. Catalyst and Sample Preparation

The Fe-TiO_2 nanoparticle was prepared by dissolving 5 mg of TiO_2 nanoparticles in 15 mL of distilled water and 2 mg of $FeCl_3$ (after grinding it) and stirring so that iron chloride would uniformly spread in the mixture. The previous solution was stirred at 500 rpm with a magnetic stirrer for 4 hours. Expose the mixture to bath ultrasonication for 30 minutes at 40 KHz, accompanied by a three-minute pause after every five minutes of ultrasonication. The sample is filtered and dried in the furnace at 110 ^{o}C for 90 min, then calcination at 450 ^{o}C for two hours and cooling. The produced nanocatalyst powders (Fe-TiO_2 composite) were analyzed using several methods to determine the presence of iron in addition to TiO_2; these analyses were published in previous work [26].

The BTX sample was prepared by adding dissolving equal amounts of 600 mg of benzene, toluene, and xylene in one liter of distilled water and then treated to ultrasonic treatment for thirty minutes. This was done in order to create roughly 600 mg/L of the wastewater. Through the addition of HCl for acidity and NaOH for alkalinity, the pH value of the solution was altered to obtain the desired effect.

2.4. Method and Measurement

After preparing the BTX solution, Fe- TiO_2 nanopowder was added at mg/L. The prepared mixture was transferred to the test section. The experiments were done under different air and water flow rates (range 0–3 L/min and 160–600 L/h, respectively), pH 6.5, and irradiation time (0, 30, 60, 90, 120) min. Each experiment was conducted three times to obtain accurate readings

4 mL of the tested samples were taken at constant intervals and measured for COD. Samples were collected after each irradiation period to measure the removal percentages. The tests were conducted in compliance with the environmental regulations of Iraq, which set the permissible COD limit at 100 ppm, according to the provisions of Law No. 25 of 1967 Concerning the Conservation of Public Water and Rivers, respectively.

The COD test uses an indirect method to assess the concentration of organic chemicals in water. COD is commonly used as an effective indicator of water quality to count the number of organic contaminants in a given sample. The oxygen mass utilized per liter of solution is typically measured in milligrams per liter (mg/L) or parts per million (ppm). COD is a key indicator for assessing the level of contamination in industrial effluent. It refers to the amount of oxygen required to chemically oxidize the oxidizing substances, particularly those in industrial waste. The concept of COD is based on biochemical processes that oxidize organic molecules, which are essential for determining the extent of organic pollution in the effluent [27]. In the COD evaluation method, the American Public Health Association (APHA), American Water Works Association (AWWA), and Water Environment Federation (WEF) utilizing potassium hydrogen phthalate (KHP) represent the organic material in the analysis. The test portion is refluxed in the existence of Hg^{2+} sulfate, along with a specified quantity of $K_2Cr_2O_7$ and silver sulfate (Ag_2SO_4) catalyst in concentrated sulfuric acid for 2 hours. During this process, part of the dichromate is reduced by the presented oxidizable material [28]. The following Eq. (1) describes the reaction that occurs when KHP is exposed to $K_2Cr_2O_7$:

$$2KC_8H_5O_4 + 10K_2Cr_2O_7 + 41H_2SO_4 \rightarrow 16CO_2 + 46H_2O + 10Cr2(SO4)3 + 11K_2SO_4 \qquad (1)$$
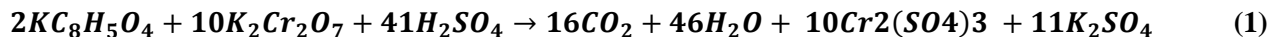
when $K_2Cr_2O_7$ is substituted by O_2, the Eq. (1) becomes Eq. (2)

$$2KC_8H_5O_4 + 15O_2 + H_2SO_4 \rightarrow 16CO_2 + 6H_2O + K_2SO_4 \qquad (2)$$
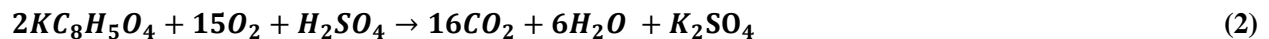
After digestion, the remaining unreduced dichromate is quantified through potentiometric titration using a Fe^{2+} solution based on the following Eq. (3):

$$Cr_2O_{72}^+ + 6Fe^{3+} + 14H^+ \rightarrow 2Cr_3^+ + 6Fe^{3+} + 7H_2O \qquad (3)$$
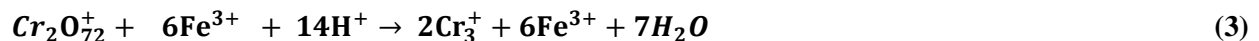
3. Results and Discussion
3.1. Influence of Photocatalysis Operating Conditions

The rates of oxidation of the photocatalytic system are impacted by various factors, including the solution's gas flow rate, liquid flow rate, pH, light intensity, catalyst loading, irradiation period, and photoreactor pollutant level. Pollutant elimination efficiency measures photocatalytic activity.

The COD removal percentage (or efficiency in R) was calculated by collecting and evaluating data under various conditions, with the parameter R acting as the analytical instrument, as shown in Eq. (4).

$$\boldsymbol{Removal\ efficiency}\ \% = (\boldsymbol{Ci} - \boldsymbol{Ct})\ \boldsymbol{Ci}/\ \times \boldsymbol{100} \qquad (4)$$

Where Ci represents the pollutant's starting concentration in ppm and Ct represents the concentration at various time intervals.

To examine the photodegradation efficiency of the developed catalyst. Experiments were conducted to investigate the efficacy of BTX removal using pure TiO_2 and doped Fe-TiO_2 at pH 6.5, catalyst dose of 50 mg/L, and light intensity of 42 W. Fig. 3 demonstrates that the clearance rate in Fe-doped TiO_2 is 50% more than that of pure titanium dioxide. Iron creates a new energy level for transition metal ions between TiO_2's valence and conducted bands. Our previous work [26] presents a comprehensive comparison of the findings between pure titanium dioxide and Fe-doped TiO_2, as well as the influencing variables on the removal efficacy of organic pollutants.
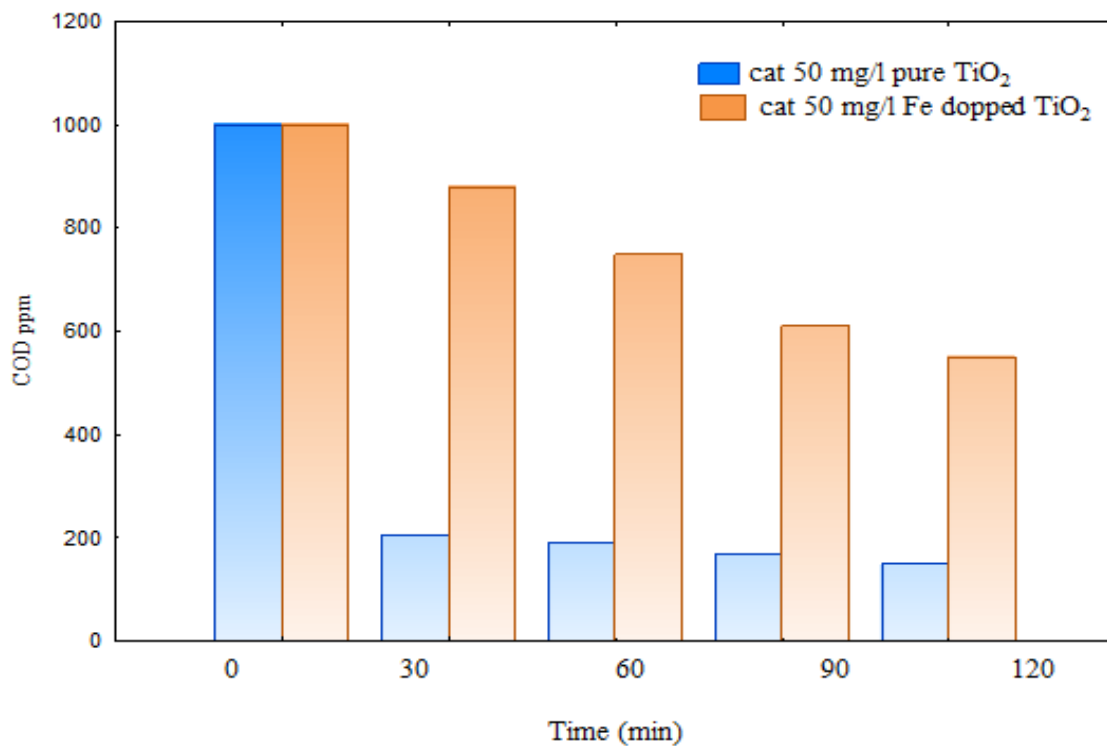
Figure 3: Comparison of pure and Fe-doped TiO_2 on BTX degradation efficiency at 50 mg/L.

3.2. Effect of Gas Flow Rate on the Removal Percentage

Fig. 4 illustrates the affections velocity of air flow on BTX photodegradation under constant liquid flow rate settings of 200 L/hr, PH (6.5), catalyst loading of 50 mg/L, and a light intensity of 200 watts.
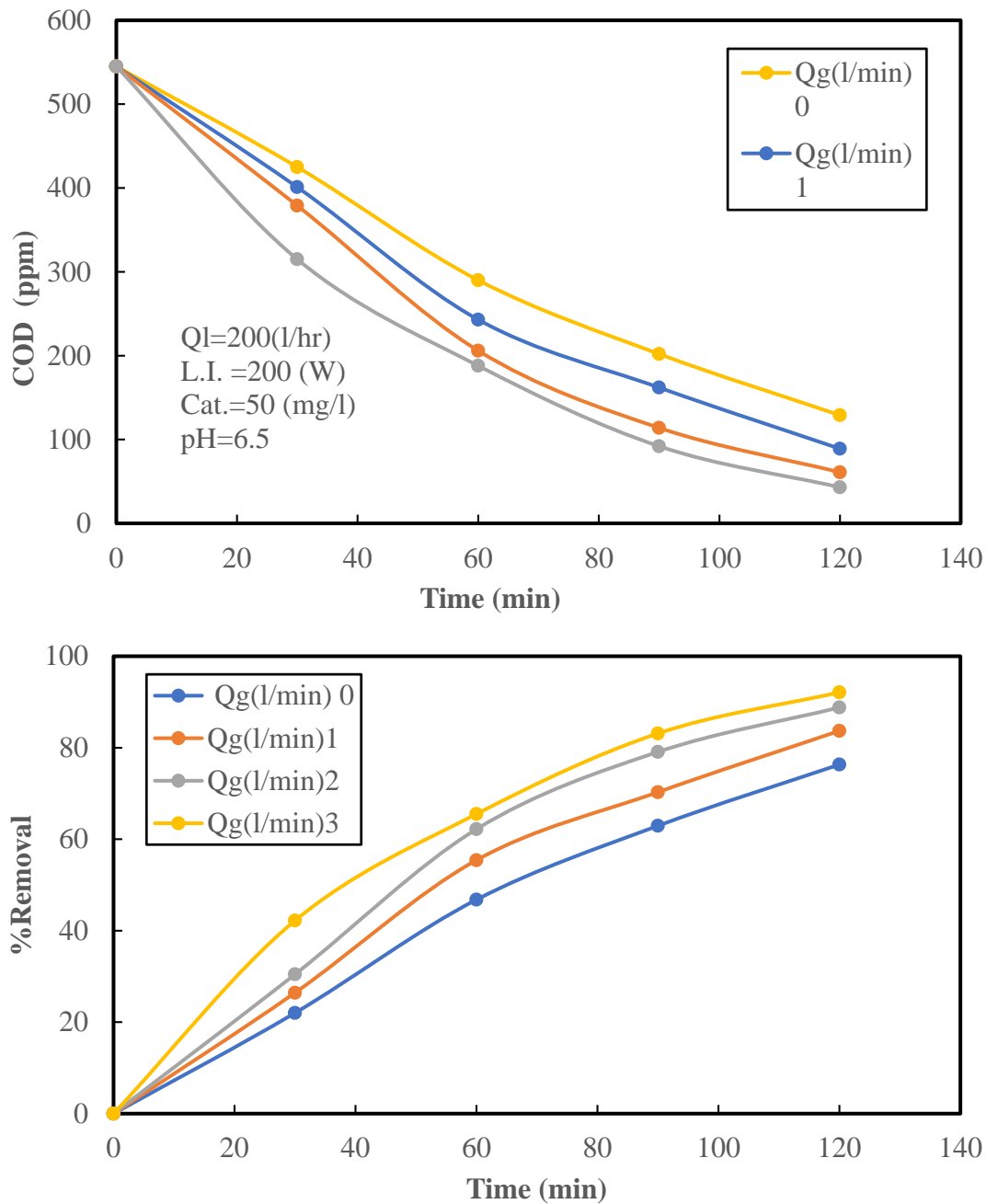
Figure 4: Correlation between irradiation duration and COD, elimination % of BTX at various gas flow rates at pH=6.5, QL=200L/hr, Cat.L.=50mg/L, and L.I.=200W.

When the airflow rate is increased under continuous testing settings, the findings indicate a considerable rise in the fraction of BTX that is removed. Under ideal circumstances, which included a pH of 6.5, a light intensity of 200 W, and a catalyst loading of 50 mg/L, it was possible to obtain a removal efficiency of BTX that was 98%. Over 120 minutes, the airflow rate of 3 liters per minute was found to have the maximum removal rate. In addition, the experiment demonstrated that the removal rate is often low and even constant when no air is present in the system. This suggests a longer period is required for a high removal rate. There are two reasons why an increased gas flow rate is beneficial to removing BTX. The first reason is that a high velocity increases the diffusion of BTX molecules to the catalyst's active sites, which in turn causes the degradation rate to speed up. The existence of rising air bubbles functions as a promoter by bringing in molecular oxygen, which is regulated by the airflow rate. This is the second component that plays a role in the process. When the catalyst's surface is illuminated by LED

light, the oxygen molecules interact with the free electrons created at the active areas using the catalyst. This is in accordance with the hypothesized process of degradation shown in Fig. 5, which results in the production of additional hydroxyl radicals, as shown in Eq. (5-12) [29].
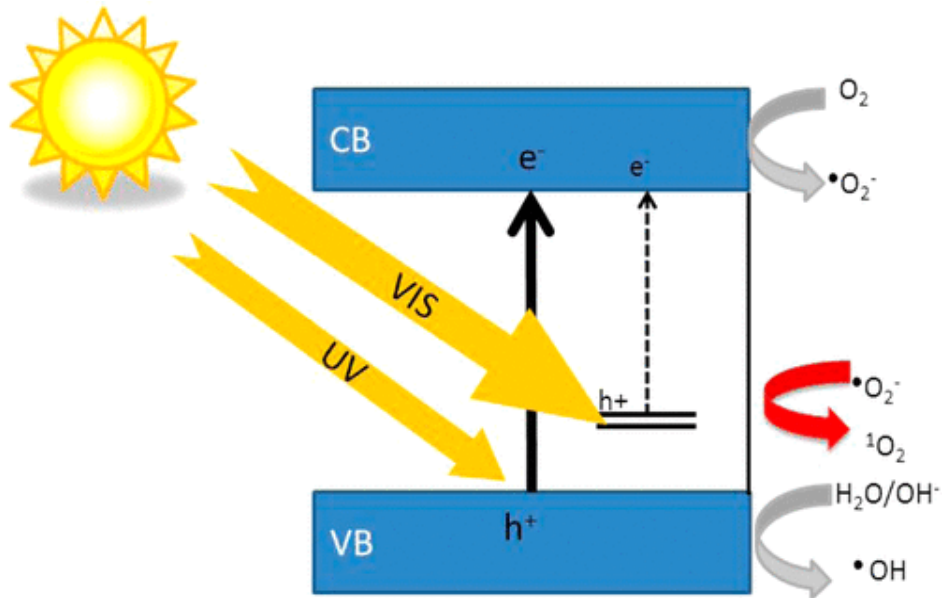
Figure 5: The photocatalysis mechanism by a visible light source [30].

$$TiO_2 + \Delta Egab\ (UV) \rightarrow TiO_2(eCB^- + hVB^+) \tag{5}$$

$$TiO_2\ (hVB^+) + H_2O \rightarrow TiO_2 + H + \ +OH \tag{6}$$

$$TiO_2\ (hVB^+) + OH \rightarrow TiO_2 + OH^{.} \tag{7}$$

$$TiO_2\ (eCB^-) + O_2 \rightarrow TiO_2 + O_2^{.-} \tag{8}$$

$$O_2^{.-} + H^+ \rightarrow HO_2^{.} \tag{9}$$

$$2HO_2^{.} \rightarrow H_2O_2 + O_2 \tag{10}$$

$$H_2O_2 + e^- \rightarrow OH^- + OH^{.} \tag{11}$$

$$BTX + OH^{.} \rightarrow degradation\ products \tag{12}$$
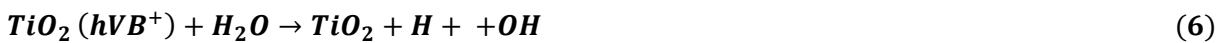
Therefore, it's evident that the flow rate affects how the contaminant degrades and is removed. The more quickly an environmental constraint may be scoped and the shorter the time required, the higher the flow rate

3.3. Effect of Circulating Liquid Flow Rate
In the photocatalytic reactor, the liquid flow rate is another very important factor that plays a significant role in determining how well BTX is removed. In order to investigate the effect that the flow rate of the liquid has on the effectiveness of BTX removal, a range of flow rates ranging from 160 to 600 liters per hour was used. At a liquid flow rate of 600 liters per hour and a gas flow rate of three liters per minute for half an hour, the most significant removal efficiency of ninety percent was achieved. The efficacy of removing BTX from a given volume of test solution may be anticipated to increase proportionally with the length of exposure to the photocatalytic surface. This is because the BTX will have a more significant number of opportunities to adsorb and oxidize at active sites when the residence time is longer.

The removal efficiency may be higher in a circulating reactor with a more significant liquid flow rate, as shown

in Fig. 6, 7, 8 and 9. This is because when the fluid flow rate is raised, there is an increase in the amount of light exposed to the wastewater, which increases the removal efficiency of BTX. This discovery is comparable to [31] [32]. At the same time, in a continuous system, the resident time and removal effectiveness can be lowered because the flow rate is heavily impacted by the resident time and the form of the penetration curve [33].
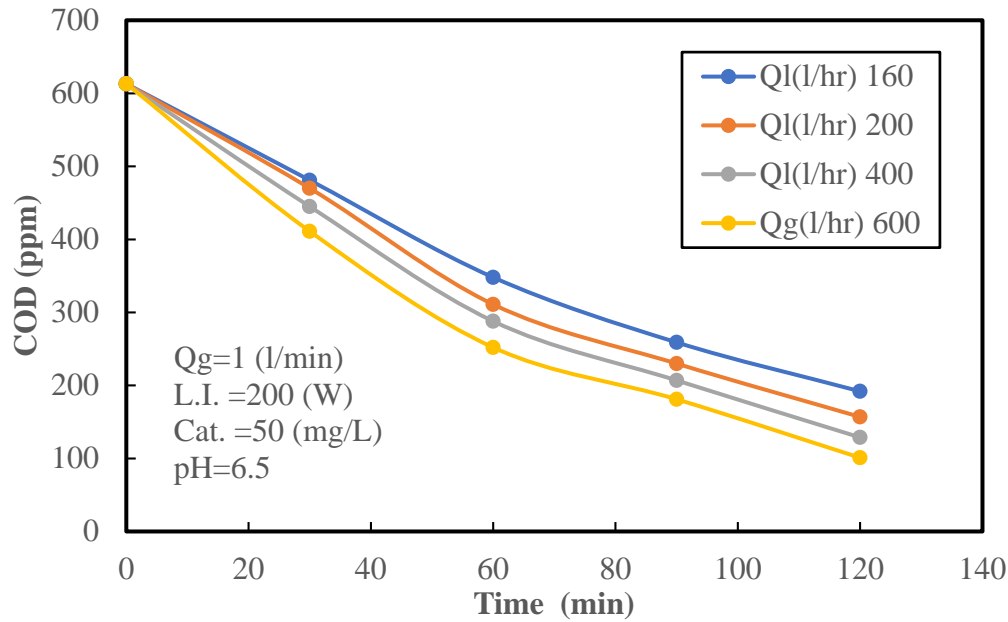
Figure 6: Correlation between time and COD at different liquid flow rates (Qg=1L/min).
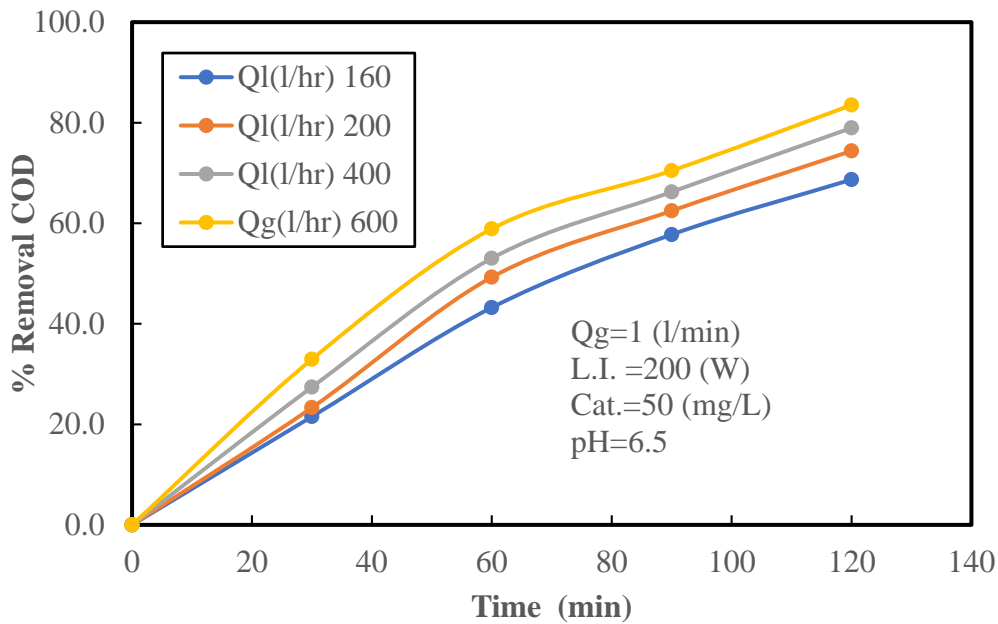
Figure 7: Correlation between time and removal percentage of BTX at different liquid flow rates (Qg=1L/min).
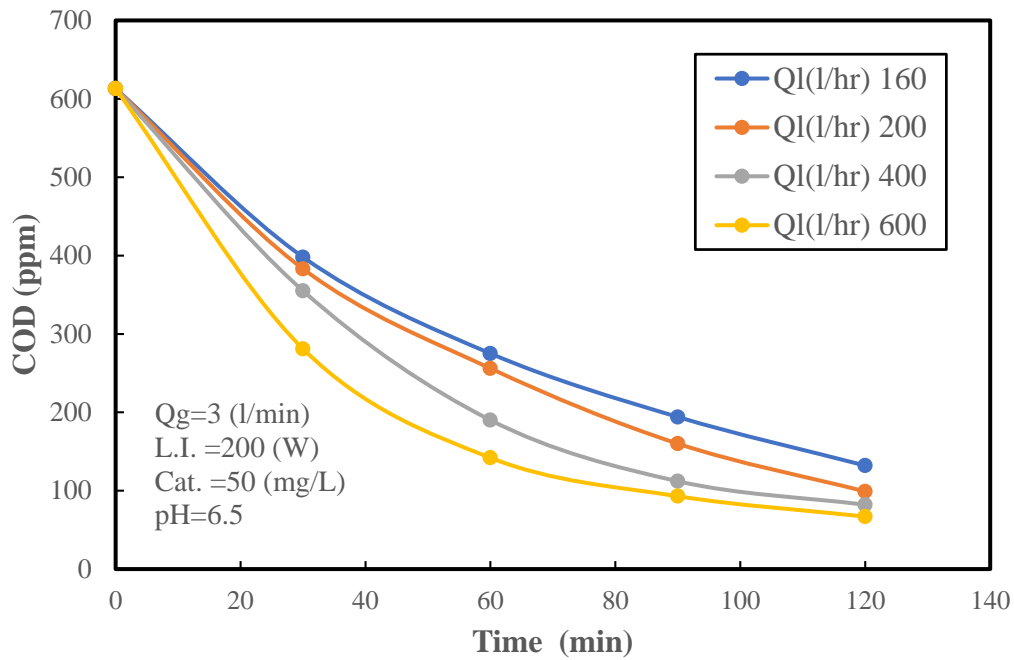
Figure 8: Correlation between time and COD at different liquid flow rate (Qg=3L/min).
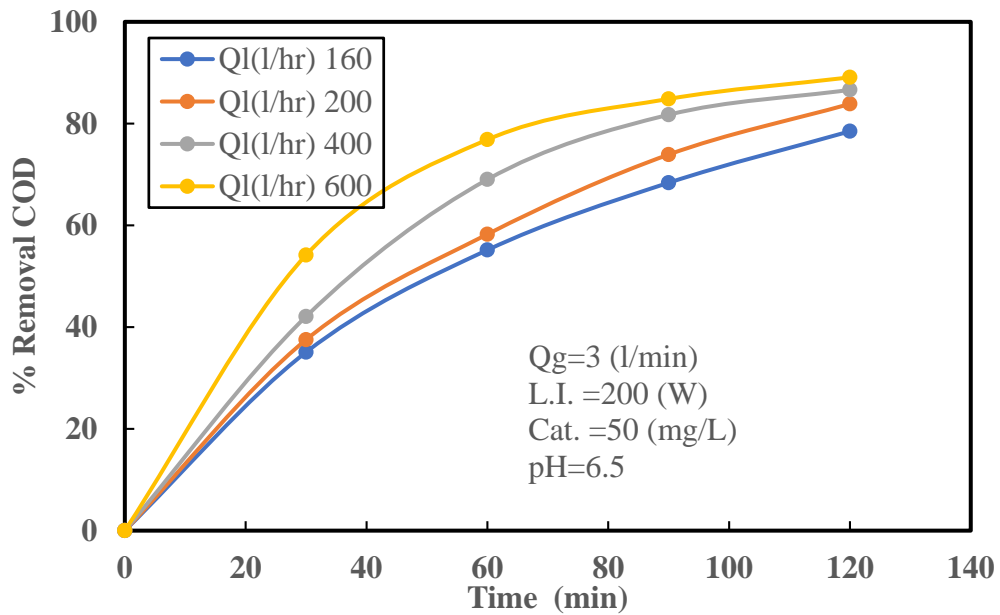
Figure 9: Correlation between time and COD, removal percentage of BTX at different liquid flow rates (PH=6.5, Qg=3L/min, Cat.L.=50mg/L and L.I.=200W).

3.4. Kinetic Study of Batch Circulating Experiments in Tapered Bubble Column

Determining the kinetic coefficients of a reaction is crucial for designing an appropriate reactor. The photocatalytic processes involved in degrading petroleum wastewater are highly complex due to the formation of numerous intermediates and final products [34].

In the progressed oxidation process, the degradation of organic compounds and their by-products through hydroxyl radical attack followed first-order kinetics concerning COD decay. In contrast, the concentration of hydroxyl radicals remained constant throughout the process [35].

Lagergren's pseudo-first-order model is the most used and easy kinetic model. The generic formulation for this model is given in Eq. (13) [36]:

$$\frac{dqt}{dt} = k1(qe - qt) \tag{13}$$

At equilibrium and at any time t (min), the adsorbate uptake rate per mass of adsorbent is provided by qe and qt, respectively. On the other hand, the constant rate of the PFO (pseudo-first order) equation is denoted by k1 (min^{-1}) in the equation.

Eq. (13) might be integrated to get the linear equation that is shown in Eq. (14) and Eq. (15) for the boundary conditions (t = 0, qt = 0 and t = t, qe = qt):

$$\ln[qe - qt] = -k1t + \ln qe \tag{14}$$

$$\ln(qe - qt)/qe = -k1\,t \tag{15}$$

Which may be rearranged in a non-linear way in Eq. (16):

$$qt = qe\,(1 - e^{-K1t}) \tag{16}$$

Pseudo-first-order kinetics has been effectively used to characterize the kinetics of numerous photocatalytic processes involving aquatic organics. The gas flow rate is the most critical component in this process.

The kinetics were examined at three Qg levels (0, 1, 2 and 3) using 50 mg/L Fe-TiO$_2$ and a duration of 120 minutes. Fig. 10 depicts the degradation of COD with time for LED/Fe-TiO$_2$ at different gas flow rate levels. For various Qg values, generally follows an almost exponential trend.
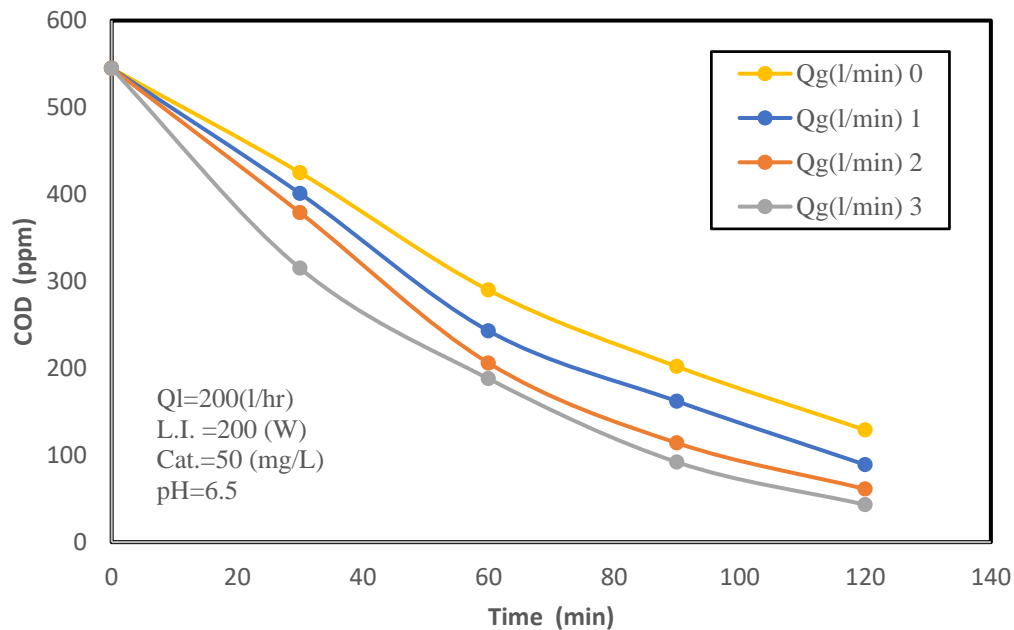
Figure 10: COD decay with time using LED/Fe-TiO$_2$ at different Qg.

Fig. 11 shows the adsorbent's adsorption capacity vs. time. Adsorption capacity was found to increase almost linearly with time and flow rate. This might be due to the attachment of additional molecules to the accessible active sorption sites during a prolonged interaction. The complete adsorption process occurred in many steps, and the most advantageous kinetic model was determined to be pseudo-first order, with R² = 0.9914, 0.9895, 0.9923,

and 0.9924 at flow rates of 0, 1, 2, and 3 L/min, respectively. Adsorption happens due to the existence of two components in the adsorption system: the pollutant and the adsorbent. When partial diffusion occurs via the pores in the adsorption process, the correlation between the initial solute concentration BTX and the rate of velocity of the substance is a linear relationship [32]. Fe-doped TiO_2 is classified as an adsorbent surface due to its capacity to generate complexes on its surface. The exact nature of the surface complex at the final state remains unknown; however, numerous practical hypotheses and predictions are discussed in the literature. The process is initially very fast but gradually slows down until reaching equilibrium [37].
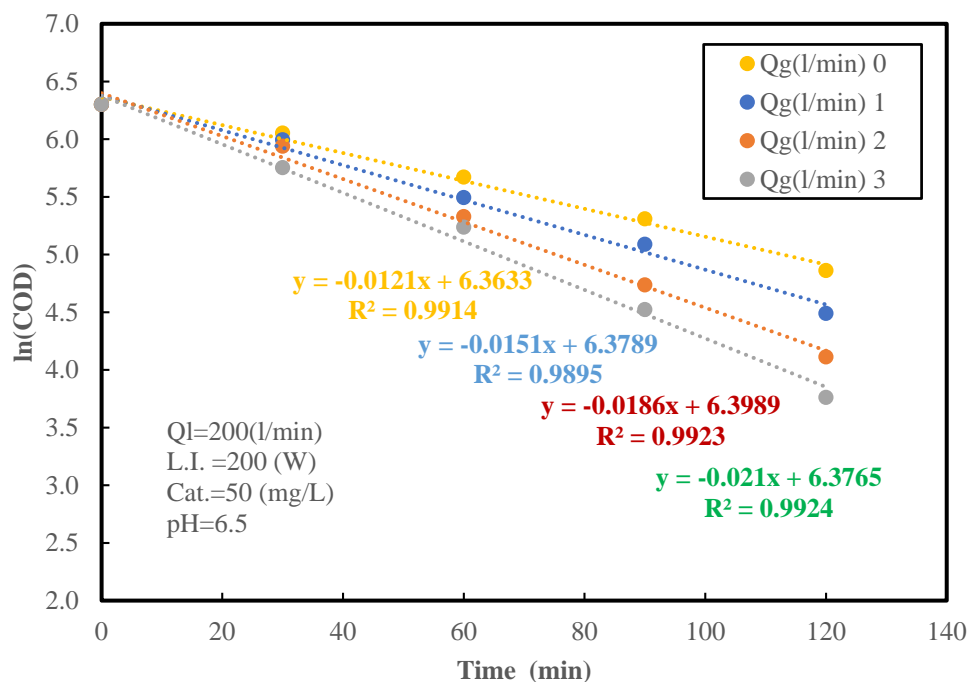
Figure 11: Pseudo first-order fitting of the photocatalytic degradation of BTX under various gas flow rates.

4. Conclusions

This work employs LED/ TiO_2 and LED/Fe-TiO_2 in circulating up-flow photocatalyst reactors to degrade BTX in produced wastewater efficiently. The results show that using dopped Fe-TiO_2 increases the COD removal by 50% more than pure TiO_2. The study declares that increasing air and water velocities increases the COD removal. The maximum reduction in chemical oxygen demand (COD) of more than 92% was achieved after 100 min and 98% removal after 2 hours of irradiation at a gas flow rate of 3 l/min, with constant pH = 6.5, light intensity =200 watts and catalyst loading = 50 mg/L. The kinetic study of the photocatalytic degradation of BTX at different gas velocities operating conditions follows a pseudo-first order model.

Conflict of Interest
The authors declare that they have no conflict of interest.

References
[1] F. M. Abdulla, Z. Y. Shnain, A. A. Alwasiti, M. F. Abid, and N. H. Abdurahman, "Photocatalysis technology for treating petroleum wastewater and the potential application of tapered bubble column (TBC): a review," 2024.
[2] S. Varjani, G. Kumar, and E. R. Rene, "Developments in biochar application for pesticide remediation: current knowledge and future research directions," *J. Environ. Manage.*, vol. 232, pp. 505–513, 2019.
[3] M. Al-Nuaim, A. A. Al-Wasiti, Z. Y. Shnain, and A. K. Al-Shalal, "The combined effect of bubble and photo catalysis technology in BTEX removal from produced water," *Bull. Chem. React. Eng. Catal.*, vol. 17, no. 3, pp. 577–589, 2022.
[4] A. Kaur, A. Umar, and S. K. Kansal, "Heterogeneous photocatalytic studies of analgesic and non-

steroidal anti-inflammatory drugs," *Appl. Catal. A Gen.*, vol. 510, pp. 134–155, 2016.

[5] Y. Li, Y. Ma, K. Li, S. Chen, and D. Yue, "Photocatalytic reactor as a bridge to Link the commercialization of photocatalyst in water and air purification," *Catalysts*, vol. 12, no. 7, p. 724, 2022.

[6] W. F. Elmobarak, B. H. Hameed, F. Almomani, and A. Z. Abdullah, "A review on the treatment of petroleum refinery wastewater using advanced oxidation processes," *Catalysts*, vol. 11, no. 7, p. 782, 2021.

[7] I. J. Ani, U. G. Akpan, M. A. Olutoye, and B. H. Hameed, "Photocatalytic degradation of pollutants in petroleum refinery wastewater by TiO_2-and ZnO-based photocatalysts: recent development," *J. Clean. Prod.*, vol. 205, pp. 930–954, 2018.

[8] D. Aljuboury, P. Palaniandy, H. B. Abdul Aziz, and S. Feroz, "Treatment of petroleum wastewater by conventional and new technologies-A review," *Glob. Nest J*, vol. 19, no. 3, pp. 439–452, 2017.

[9] D. K. Dubey, D. N. Singh, S. Kumar, C. Nayak, P. Kumbhakar, S. N. Jha, *et al.*, "Local structure and photocatalytic properties of sol–gel derived Mn–Li co-doped ZnO diluted magnetic semiconductor nanocrystals," *RSC Adv.*, vol. 6, no. 27, pp. 22852–22867, 2016.

[10] Y. Zhang, Y. Shen, F. Gu, M. Wu, Y. Xie, and J. Zhang, "Influence of Fe ions in characteristics and optical properties of mesoporous titanium oxide thin films," *Appl. Surf. Sci.*, vol. 256, no. 1, pp. 85–89, 2009.

[11] O. Sacco, D. Sannino, M. Matarangolo, and V. Vaiano, "Room temperature synthesis of V-doped TiO_2 and its photocatalytic activity in the removal of caffeine under UV irradiation," *Materials (Basel).*, vol. 12, no. 6, p. 911, 2019.

[12] S. Chatrnoor, A. H. Taghadossi, S. A. A. Alem, F. Taati-Asil, B. Raissi, R. Riahifar, *et al.*, "Synthesizing Fe-Doped TiO_2 Nanoparticles by Anodic Dissolution Method and Preparing An Electrophoretic Deposited Layer," *Available SSRN 4369392*.

[13] N. L. Heda, K. Kumar, V. Sharma, U. Ahuja, S. Dalela, and B. L. Ahuja, "Impact of Co doping on electronic response, momentum densities and localisation of d electrons of TiO_2: Compton profiles and first-principles calculations," *Mater. Today Commun.*, vol. 34, p. 105144, 2023.

[14] A. P. Singh, N. Kodan, B. R. Mehta, A. Held, L. Mayrhofer, and M. Moseler, "Band edge engineering in $BiVO_4/TiO_2$ heterostructure: enhanced photoelectrochemical performance through improved charge transfer," *ACS Catal.*, vol. 6, no. 8, pp. 5311–5318, 2016.

[15] Y.-H. Peng, G.-F. Huang, and W.-Q. Huang, "Visible-light absorption and photocatalytic activity of Cr-doped TiO2 nanocrystal films," *Adv. Powder Technol.*, vol. 23, no. 1, pp. 8–12, 2012.

[16] P. B. Nair, V. B. Justinvictor, G. P. Daniel, K. Joy, V. Ramakrishnan, D. D. Kumar *et al.*, "Structural, optical, photoluminescence and photocatalytic investigations on Fe doped TiO_2 thin films," *Thin Solid Films*, vol. 550, pp. 121–127, 2014.

[17] L. G. Devi, P. M. Nithya, C. Abraham, and R. Kavitha, "Influence of surface metallic silver deposit and surface fluorination on the photocatalytic activity of rutile TiO_2 for the degradation of crystal violet a cationic dye under UV light irradiation," *Mater. Today Commun.*, vol. 10, pp. 1–13, 2017.

[18] M. Manzoor, A. Rafiq, M. Ikram, M. Nafees, and S. Ali, "Structural, optical, and magnetic study of Ni-doped TiO_2 nanoparticles synthesized by sol–gel method," *Int. Nano Lett.*, vol. 8, pp. 1–8, 2018.

[19] M. B. Marami, M. Farahmandjou, and B. Khoshnevisan, "Sol–gel synthesis of Fe-doped TiO_2 nanocrystals," *J. Electron. Mater.*, vol. 47, pp. 3741–3748, 2018.

[20] Z. Xu, C. Li, N. Fu, W. Li, and G. Zhang, "Facile synthesis of Mn-doped TiO_2 nanotubes with enhanced visible light photocatalytic activity," *J. Appl. Electrochem.*, vol. 48, pp. 1197–1203, 2018.

[21] T. P. Oliveira, S. F. Rodrigues, G. N. Marques, R. C. Viana Costa, C. G. Garçone Lopes, C. Aranas Jr, *et al.*, "Synthesis, characterization, and photocatalytic investigation of $CuFe_2O_4$ for the degradation of dyes under visible light," *Catalysts*, vol. 12, no. 6, p. 623, 2022.

[22] A. O. Ibhadon and P. Fitzpatrick, "Heterogeneous photocatalysis: recent advances and applications," *Catalysts*, vol. 3, no. 1, pp. 189–218, 2013.

[23] R. Ahmad, Z. Ahmad, A. U. Khan, N. R. Mastoi, M. Aslam, and J. Kim, "Photocatalytic systems as an advanced environmental remediation: Recent developments, limitations and new avenues for applications," *J. Environ. Chem. Eng.*, vol. 4, no. 4, pp. 4143–4164, 2016.

[24] A. E. Cassano and O. M. Alfano, "Reaction engineering of suspended solid heterogeneous

photocatalytic reactors," *Catal. today*, vol. 58, no. 2–3, pp. 167–197, 2000.

[25] R. L. Pozzo, R. J. Brandi, J. L. Giombi, A. E. Cassano, and M. A. Baltanás, "Fluidized bed photoreactors using composites of titania CVD-coated onto quartz sand as photocatalyst: Assessment of photochemical efficiency," *Chem. Eng. J.*, vol. 118, no. 3, pp. 153–159, 2006.

[26] F. M. Abdulla, Z. Y. Shnain, A. A. Alwaisit, and M. F. Abid, "Use of Synthetic Iron Oxide-Doped Titanium Dioxide Nanoparticles in Photocatalytic Degradation of BTX from Petroleum Wastewater," *Russ. J. Appl. Chem.*, 2024.

[27] A. C. Bader, H. J. Hussein, and M. T. Jabar, "BOD: COD ratio as Indicator for wastewater and industrial water pollution," *Int. J. Spec. Educ*, vol. 37, no. 3, pp. 2164–2171, 2022.

[28] R. B. Geerdink, R. S. van den Hurk, and O. J. Epema, "Chemical oxygen demand: Historical perspectives and future challenges," *Anal. Chim. Acta*, vol. 961, pp. 1–11, 2017.

[29] S. Banerjee, S. C. Pillai, P. Falaras, K. E. O'shea, J. A. Byrne, and D. D. Dionysiou, "New insights into the mechanism of visible light photocatalysis," *J. Phys. Chem. Lett.*, vol. 5, no. 15, pp. 2543–2554, 2014.

[30] M. F. Abid, S. T. Hamiedi, S. I. Ibrahim, and S. K. Al-Nasri, "Removal of toxic organic compounds from synthetic wastewater by a solar photocatalysis system," *Desalin. Water Treat.*, vol. 105, pp. 119–125, 2018.

[31] M. F. Abid, O. N. Abdulla, and A. F. Kadhim, "Study on removal of phenol from synthetic wastewater using solar photo catalytic reactor," *J. King Saud Univ. - Eng. Sci.*, vol. 31, no. 2, pp. 131–139, 2019.

[32] S. Hekmat, "Thermodynamic and Kinetic Study of Adsorption of Azo Dyes Derived for 4-amino Anti pyrene by Activated Carbon," *J. Educ. Sci.*, vol. 29, no. 2, pp. 63–81, 2020.

[33] S. Mozia, M. Tomaszewska, and A. W. Morawski, "Photodegradation of azo dye Acid Red 18 in a quartz labyrinth flow reactor with immobilized TiO_2 bed," *Dye. Pigment.*, vol. 75, no. 1, pp. 60–66, 2007.

[34] F. Shahrezaei, Y. Mansouri, A. A. L. Zinatizadeh, and A. Akhbari, "Process modeling and kinetic evaluation of petroleum refinery wastewater treatment in a photocatalytic reactor using TiO_2 nanoparticles," *Powder Technol.*, vol. 221, pp. 203–212, 2012.

[35] H. Öztürk, S. Barışçı, and O. Turkay, "Paracetamol degradation and kinetics by advanced oxidation processes (AOPs): Electro-peroxone, ozonation, goethite catalyzed electro-fenton and electro-oxidation," *Environ. Eng. Res.*, vol. 26, no. 2, 2021.

[36] H. Moussout, H. Ahlafi, M. Aazza, and H. Maghat, "Critical of linear and nonlinear equations of pseudo-first order and pseudo-second order kinetic models," *Karbala Int. J. Mod. Sci.*, vol. 4, no. 2, pp. 244–254, 2018.

[37] A. M. Kadhum, S. A. Mohammed, D. H. Attol, and E. A. A. A. Alshawi, "Kinetic Study of Adsorption of Murexide Dye Polluting the Aquatic Environment Using one of the Industrial Wastes, Antimony Trioxide, and its Applicability to Freundlich Isotherm" *International Journal of Drug Delivery Technology*, vol. 12, no. 2, pp. 490-494, 2022.